The Cryosphere Discussions

Modeling the thermal dynamics of the active layer at two contrasting permafrost sites

J. Weismüller[1,*], U. Wollschläger[1,], J. Boike[2], and K. Roth[1]**

[1]Institute of Environmental Physics, Heidelberg University, Im Neuenheimer Feld 229, 69120 Heidelberg, Germany
[2]Alfred Wegener Institute for Polar and Marine Research – Research Unit Potsdam, Telegrafenberg A 43, 14473 Potsdam, Germany
[*]now at: Department of Earth and Environmental Sciences, Geophysics Section, Ludwig-Maximilians University, Theresienstr. 41, 80333 Munich, Germany
[**]now at: UFZ – Helmholtz Centre for Environmental Research, Permoserstraße 15, 04318 Leipzig, Germany

Correspondence to: K. Roth (kurt.roth@iup.uni-heidelberg.de)

Title Page

Abstract	Introduction
Conclusions	References
Tables	Figures

|◄ | ►|
| ◄ | ► |

| Back | Close |

Full Screen / Esc

Printer-friendly Version

Interactive Discussion

Modeling thermal dynamics of active layers

J. Weismüller et al.

Abstract

The thermal and hydraulic dynamics of unsaturated active layers are described in a one-dimensional numerical forward model. Hydraulic and thermal transport processes are coupled in a set of partial differential equations based on Richards' equa-
5   tion, conductive and convective heat flow and a phenomenological description of soil freezing. The model is applied to the detailed data sets of two rather different field sites, one in the Arctic on Svalbard and one on the Tibetan Plateau. Soil temperatures and water contents as well as important quantities like the thaw depth and the duration of the isothermal plateau can be reproduced. To examine the influence of different
10   heat transport processes, three scenarios of different complexity are studied. We show that heat conduction is the dominant process at both sites. While representing this process is sufficient for rough thaw depth estimates, a more detailed representation is necessary for an accurate representation of the active layer thermal dynamics. With our detailed model, characteristic deviations between measurements and simulations
15   can still be observed. As possible explanations we discuss downward vapor migration in the upper soil layer and mechanical deformations.

1   Introduction

Permafrost soils are present on about one fifth of the Earth's land surface (French, 2007), and the processes that take place in these regions are of great importance for
20   understanding the local environment as well as the global climatic conditions. The upper part of the permafrost, which undergoes seasonal freeze and thaw, the active layer, is where almost all of the biologic and hydrological processes take place. It is therefore crucial to obtain a quantitative understanding of the thermal and hydraulic dynamics of this layer in order to predict the consequences of climatic change on the
25   active layer and the underlying permafrost.

One approach to quantitatively study the processes taking place in the active layer of permafrost soils is the application of analytical and numerical models. The most widely applied analytical approach to soil freezing and thawing is based on the Stefan's problem, which yields a sharp thawing front (Javierre et al., 2006). Nakano and Brown (1971) suggested the incorporation of a finite freezing zone instead of a sharp freezing front into this model to account for the unfrozen water that may be present at sub-zero temperatures. They included latent heat as an effective heat capacity within the freezing zone, and presented a numerical scheme for the solution. Harlan (1973) coupled Richards' equation with the heat equation based on Fourier's law and solved it using a finite difference scheme, observing movement of water and heat from warm to cold regions. Guymon and Luthin (1974) presented a very similar model and solved it using a finite element scheme. Engelmark and Svensson (1993) proposed a solution scheme based on finite volumes that solves directly for the ice and water content and successfully checked the results against laboratory measurements. Hinzman et al. (1998) used a one dimensional subsurface model for simulating heat conduction and solved it with a one dimensional finite element scheme. They coupled this with a surface heat balance model to predict the thaw depth of the Kuparuk River watershed on the North Slope of Alaska from meteorologic data at seven stations, obtaining good results. Harris et al. (2001) developed an analytical approximation for the heat transport problem in porous media, explicitly accounting for non-equilibrium processes occurring during rapid phase change. Many other modeling studies based on these approaches have been presented, of which Riseborough et al. (2008) give an extensive overview.

While many studies assume purely conductive heat transport, Kane et al. (2001) examined different non-conductive heat transport processes that can be expected in freezing soils, and assets that infiltration of liquid water can contribute significantly to soil thawing in spring. Daanen et al. (2007) worked with a three dimensional finite difference model based on the heat equation coupled with Richards' equation and used this to examine liquid water movement during freezing. Romanovsky and Osterkamp (1997) compared a model similar to the one by Guymon and Luthin (1974) with two

other commonly used models, one based on Stefan's problem and the other based on a finite difference scheme with front tracking. They determined that the physically based model similar to the one by Guymon and Luthin (1974) only returns reliable results when small time steps and high spatial resolutions are used that account for the speed at which the exterior forcing changes.

In this study we focus on the understanding of processes within the active layer. We present a physically based, coupled thermal and hydraulic model similar to the coupled models that were discussed here and perform a detailed process analysis comparing two contrasting permafrost sites: One in the Arctic on Spitsbergen, the Bayelva site (which has been described previously e.g. by Roth and Boike, 2001), and one on the Tibetan Plateau, the Tianshuihai site. The Bayelva site is a low altitude, high latitude site, while the Tianshuihai site is a high altitude, low latitude site. Climatic conditions differ significantly: at the Bayelva site, the climate is dominated by the North Atlantic Current, with humid conditions, moderate temperatures and low radiative forcing. The Tianshuihai site in contrast is dominated by continental climate in a very dry environment, high diurnal temperature variations and strong radiative forcing. At both sites, soil temperature and water content profiles have been installed, which allow the calibration of the model as well as comparison of the simulation results with ground truth.

Examining these contrasting sites we show the similarity of the thermal processes in the active layer in two rather different permafrost regions, and identify specific deviations in the model results from the measured data that can be observed at both study sites. In order to illustrate the importance of different processes, we present three different simulation scenarios in which conduction and convection by liquid water and water vapor migration are studied.

Modeling thermal dynamics of active layers

J. Weismüller et al.

Title Page

Abstract	Introduction
Conclusions	References
Tables	Figures

◁◁   ▷▷

◁   ▷

Back   Close

Full Screen / Esc

Printer-friendly Version

Interactive Discussion

J. Weismüller et al.

Title Page

Abstract	Introduction
Conclusions	References
Tables	Figures

◄ | ►

◄ | ►

Back | Close

Full Screen / Esc

Printer-friendly Version

Interactive Discussion

2 Study sites

2.1 The Bayelva site

This site and the corresponding data were described earlier, e.g. Roth and Boike (2001), Boike et al. (2003) and Boike et al. (2008), and we just repeat the pertinent features here.

The Bayelva site is located in the catchment of the Bayelva River on Svalbard, about 3 km west of Ny Ålesund at 78°55′ N, 11°50′ E (Fig. 1). In this region, the active layer is underlain by continuous permafrost that stretches out to several hundred meters in depth. Mean annual precipitation is about 400 mm, mostly falling as snow from September throughout May.

The study site is covered with unsorted, circular mud boils that have a diameter of about 1 m and are about 0.15 m high, with bare centers and low vegetation growing between them (Fig. 2).

In this study, we use daily averaged data from temperature sensors and time domain reflectometry (TDR) probes that have been installed in the center of one of these mud boils at depths as shown in Fig. 5. The accuracy of the temperature sensors was estimated to 0.02 °C over the whole temperature range observed, while the TDR measurements return soil volumetric water contents with an estimated error of 0.02 to 0.05. There is an additional sensor pair in 0.25 m depth, but the measured temperatures start drifting, so it was omitted here. The temperature sensor in 0.77 m also starts drifting by 0.1 to 0.2 °C in 2001, but has been included nevertheless due to the small extent of the deviation. We work with data starting on 14 September 1998 and ending on 2 December 2001. This is the same data set as presented by Roth and Boike (2001), with an additional year.

Within the instrumented mud boil the soil mainly consists of silty clay with few interspersed stones, and coal lenses occurring below 0.85 m. The average soil bulk density is 1.60×10^3 kg m^{-3}, porosity ranges from 0.36 to 0.5.

2.2 The Tianshuihai site

The Tianshuihai site is located on the Tibetan Plateau in the Aksai Chin Region, Xin-jiang Uigur Autonomous Region, W-China at 35 °24′ N, 79°33′ E (Fig. 1). In this region, a vast plain stretches out at 4740 m above sea level, framed by mountains (Fig. 3). At the location of the site, the permafrost extends down to 75 to 120 m depth (Li and He, 1989).

Due to its low geographical latitude, the Tibetan Plateau contains the only large permafrost region on Earth that is exposed to strong daily fluctuations in the radiative forcing. Measurements recorded at the Tianshuihai climate station, which was installed in September 2007, ranged from $-100\,\mathrm{W\,m}^{-2}$ at night to more than $800\,\mathrm{W\,m}^{-2}$ in June 2008, while daily averages mostly stay between 0 and $150\,\mathrm{W\,m}^{-2}$. Measured air temperatures ranged from $-8\,°C$ to $21\,°C$ in July 2008 and from $-38\,°C$ to $-5\,°C$ in January 2009. With about $24\,\mathrm{mm\,y}^{-1}$ of rain (Li and He, 1989), precipitation is very low in this region.

The plain area around the study site is characterized by loamy ridges of several centimeters in height which alternate with patches consisting of gravel and sand (Fig. 3). At the top of the ridges characteristic cracks occur. They are filled with sand wedges and indicate considerable frost action at this site. There is no vegetation present in the region.

In this study, we use soil temperature and soil water content data from a profile of about 1.75 m depth which has been installed as part of the Tianshuihai climate station and reaches about 0.2 m into the permafrost. It is located in a patch of gravel and sand in the center of a trough which is framed by loamy rims. The upper ten to fifteen centimeters consist of fine sand and some gravel, followed by a layer of sand and gravel that extends down to about one meter depth, which is then underlain by a layer of loam with interspersed patches of gravel. Porosities, densities, heat capacities and hydraulic and thermal properties were estimated from the recorded data or by numerical simulations.

Daily averages of soil temperatures and volumetric water contents, which were measured between 25 March 2008 and 28 December 2009, were used in this study (Fig. 6). The temperature sensors were calibrated with a relative accuracy of 0.02 °C to 0.03 °C, while for the TDR probes we assume an error of 0.02 to 0.05 in liquid water content.

3 Model description

To describe the dynamics of the active layer, we make several simplifications: we neglect mechanical processes and concentrate on heat transfer, examining heat conduction and convection by liquid water and water vapor. For this, we assume a one dimensional, initially uniform soil with an incompressible, rigid matrix.

The model is based on a modified version of Richards' equation coupled with a heat equation based on Fourier's law. To simulate soil freezing, a parameterized freezing curve was included into Richards' equation, and terms for convective heat transport by liquid water as well as a parameterized formulation for water vapor flow were introduced into the equations.

3.1 Water transport

We model the one-dimensional hydraulic dynamics based on the conservation of mass in a molar formulation,

$$\frac{\partial c_w}{\partial t} + \partial_z j_w = 0, \tag{1}$$

where c_w is the molar concentration of water with respect to the entire volume (mol m^{-3}), given by $c_w = \theta_l v_l + \theta_i v_i$. j_w is the total water flux (mol m^{-2} s^{-1}), including liquid water and water vapor. θ_l and θ_i are the volumetric contents of liquid water and ice, respectively, $v_l = \frac{\rho_l}{M_w}$ and $v_i = \frac{\rho_i}{M_w}$ the molar densities (mol m^{-3}), M_w is the molar mass of water (kg mol^{-1}), and ρ_l and ρ_i are the mass densities of liquid water and ice, both

235

set to $1000 \, \mathrm{kg\,m^{-3}}$. This assumption is necessary, because without it the change of the water density upon freezing would lead to unrealistically large gauge pressures that cannot be converted into an expansion of the soil matrix due to the lack of a mechanical model.

The water flux is given by Buckingham-Darcy's law,

$$j_w = -\nu_l K_l(\theta_l, T)(\partial_z p_w - \rho_l g), \tag{2}$$

where K_l is the liquid phase conductivity ($\mathrm{m^3\,s\,kg^{-1}}$), T the temperature (°C), g the gravitational acceleration ($\mathrm{m^2\,s^{-1}}$) and p_w the water pressure (Pa). Following Guymon and Luthin (1974) we neglect the ice pressure, assuming that both liquid water and ice pressure are given by p_w.

To relate the total water content θ_w to the water pressure p_w, we use the soil water retention curve proposed by van Genuchten (1980):

$$\theta_w = \begin{cases} \theta_r + (\phi - \theta_r) \times \left[1 + (\alpha(p_{atm} - p_w))^n\right]^{-m} & \text{if } p_w < p_{atm} \\ \phi & \text{else} \end{cases}, \tag{3}$$

where ϕ is the porosity, θ_r the residual water content, p_{atm} the atmospheric pressure (Pa), $m = 1 - \frac{1}{n}$ and α ($\mathrm{Pa^{-1}}$) and n (–) are scaling and shape parameters, respectively.

Several approaches exist to obtain the latent heat contributions to the apparent heat capacity in dependence of the total water content θ_w and the temperature T. Hansson et al. (2004) use the generalized Clapeyron equation to relate the water pressure p_w to the temperature T and model the coexistence of the liquid and solid phases by introducing an empirical relationship for the apparent heat capacity, while Hinzman et al. (1998) apply a parameterized exponential function to obtain the latent heat content of the soil in dependence of the temperature. For the study sites that are discussed in this paper we use the following empirical relationship to obtain the ice content from the total water content θ_w and the temperature T:

$$\theta_i = \begin{cases} \left[1 - \frac{1}{\phi}\left(-\frac{a}{T-b} + cT + d\right)\right]\theta_w & \text{if } T < 0 \, ^\circ\mathrm{C} \\ 0 & \text{else} \end{cases}. \tag{4}$$

Title Page

Abstract | Introduction

Conclusions | References

Tables | Figures

◀◀ | ▶▶

◀ | ▶

Back | Close

Full Screen / Esc

Printer-friendly Version

Interactive Discussion

The parameters a, b, c and d can be used to fit this curve into the saturated branches of the soil freezing characteristic, the function that relates the liquid water content θ_l to the temperature T. In order to ensure that no ice is present at $0\,°C$ we require $b = \frac{a}{\phi - d}$, which leaves three free parameters for the ice content.

To obtain the liquid phase conductivity we use the model proposed by Mualem (1976) combined with the van Genuchten parameterization (Eq. 3),

$$K_l = \frac{\kappa}{\mu_l} \left[\frac{\theta_l - \theta_r}{\phi - \theta_r} \right]^{0.5} \left[1 - \left(1 - \left(\frac{\theta_l - \theta_r}{\phi - \theta_r} \right)^{\frac{1}{m}} \right)^m \right]^2 , \tag{5}$$

where κ is the hydraulic permeability (m^2) and μ_l the dynamic viscosity of liquid water (Pa s).

In the above formulation we assume that the decrease of the liquid water content due to freezing is equivalent to a reduction due to drainage, which implies that in the unsaturated zone ice will form preferentially at the gas–liquid interface.

3.2 Heat transport

The heat equations are based on the principle of energy conservation, which reads

$$\frac{\partial E}{\partial t} + \partial_z j_e = 0, \tag{6}$$

with the thermal energy density E (J m^{-3}) and the energy flux j_e (W m^{-2}).

Sensible heat of liquid water, ice, gas and soil matrix as well as latent heat contribute to the total thermal energy, so if we define the unfrozen soil at $0\,°C$ as reference state, we obtain

$$E = \theta_w C_l \nu_l T + (C_i \nu_i - C_l \nu_l) \int_{0\,°C}^{T} \theta_i(T') \, dT'$$

$$+ \theta_g C_g \nu_g T + (1 - \phi) C_{soil} T - L_f \theta_i \nu_i. \tag{7}$$

C_i, C_l and C_g are the molar heat capacities of ice, liquid water and gas ($\mathrm{J\,mol^{-1}\,K^{-1}}$), C_{soil} is the volumetric heat capacity of the soil matrix ($\mathrm{J\,m^{-3}\,K^{-1}}$), L_f is the latent heat of freezing ($\mathrm{J\,mol^{-1}}$) and θ_g is the volume fraction occupied by gas, given by $\theta_g = \phi - \theta_w$. The molar density of the gas v_g ($\mathrm{mol\,m^{-3}}$) is given by the ideal gas law as $v_g = \frac{p_{atm}}{R(T+273.15\,\mathrm{K})}$, with the universal gas constant R ($\mathrm{J\,mol^{-1}\,K^{-1}}$).

In Eq. (7) we included the latent heat of vaporization in the constant effective heat capacity C_g of the gas, assuming that the amount of water vapor is proportional to the temperature T. As described in the next section, this is not correct, but due to the small amount of water vapor that is present at typical temperatures in permafrost soils, the approximation seems reasonable at this place. The integral in Eq. (7) can be evaluated using Eq. (4).

When energy transport by water vapor is not considered, the energy flux can be written as

$$j_e = T C_l j_w - K_h \partial_z T. \tag{8}$$

Following de Vries (1975), the heat conductivity K_h ($\mathrm{W\,m^{-1}\,K^{-1}}$) is parameterized as

$$K_h = \frac{\sum_{\iota=1}^{4} k_\iota \theta_\iota K_{h_\iota}}{\sum_{\iota=1}^{4} k_\iota \theta_\iota}, \tag{9}$$

with the form factors k_ι (–), and the sums ranging over all constituents of the soil, namely liquid water, ice, gas and soil matrix. The k_ι describe the ratio of the average temperature gradient in particles of type ι to the average temperature gradient in the soil. If the particles are assumed to be independent spheres, the form factors are given by de Vries (1975) as

$$k_\iota = \left[1 + \frac{1}{3} \left(\frac{K_{h_\iota}}{K_{h_{soil}}} - 1 \right) \right]^{-1}, \tag{10}$$

assuming that the soil matrix forms a continuous background medium. As Ippisch et al. (1998) have shown, this approximation gives good results when compared to simulations that consider the structure of a soil sample explicitly.

3.3 Vapor transport

We implemented water vapor transport in a model following Bittelli et al. (2008) that describes water movement and latent heat transport within the soil by water vapor diffusion, including flow that is driven by vapor gradients as well as thermally driven flow. Also, we only consider thermal energy transport by latent heat and neglect sensible contributions, because the latent heat is two to three orders of magnitude larger than the sensible heat for the relevant temperatures.

When we include vapor transport, Eq. (2) is changed to

$$j_w = -v_l K_l(\theta_l, T)(\partial_z p_w - \rho_l g) + j_g, \tag{11}$$

while Eq. (8) becomes

$$j_e = T C_l j_w + L_v j_g - K_h \partial_z T, \tag{12}$$

with the latent heat of vaporization L_v ($J\,mol^{-1}$), and the molar vapor flux j_g ($mol\,m^{-2}\,s^{-1}$) given by

$$j_g = -D_g \partial_z c_v - D_g h_r s \partial_z T, \tag{13}$$

accounting for vapor flow by concentration gradients (first term) and thermally driven flow (second term).

The molar concentration of water vapor c_v ($mol\,m^{-3}$) is given by the Magnus formula (Weischet, 1991) as

$$c_v = \frac{610.78\ \text{Pa}}{R(T + 273.15\ \text{K})} \exp\left(\frac{17.08085T}{T + 234.175\ \text{K}}\right) h_r, \tag{14}$$

with the relative humidity h_r given by Philip (1957)

$$h_r = \exp\left(\frac{p_w M_w g}{R(T + 273.15\text{ K})}\right).$$ (15)

Following Bittelli et al. (2008), the water vapor diffusivity is parameterized as

$$D_g = 0.9 D_0 (\phi - \theta_w)^{2.3}\left(\frac{T}{273.15\text{ K}}\right)^{1.75},$$ (16)

with $D_0 = 2.12 \times 10^{-5}\text{ m}^2\text{ s}^{-1}$.

Using the equation of Buck (1981) for the saturation vapor pressure, the slope of the saturation vapor concentration s ($\text{mol m}^{-3}\text{ K}^{-1}$) is given by Bittelli et al. (2008) as

$$s = \frac{2.504 \times 10^6\text{ Pa K}}{p_{atm}}(T + 510.45\text{ K})^{-2}\exp\left(\frac{17.27(T + 273.15\text{ K})}{T + 510.45\text{ K}}\right)c_v.$$ (17)

3.4 Numerical solution

We solved the set of two coupled, parabolic partial differential equations for the state variables p_w and T in one dimension using the finite element software package COMSOL Multiphysics (2008). A spatial grid of 0.01 m and an adaptive time stepping with a maximum time step of 5 min was used. Solutions of the Richards' equation were compared with solutions done by SWMS (Šimůnek et al., 1995), and solutions of the heat equation including freezing were compared to analytical solutions to Stefan's problem (Carslaw and Jaeger, 1959), yielding good agreement. Mass and energy balances were checked against rain and net radiation, as these meteorological variables give an intuitive estimate for the boundary fluxes. The numerical mean daily mass defect stays below 0.71% of the average daily rain per square meter for the Bayelva scenarios, and the mean daily energy defect does not exceed 0.34%/0.09% of the average daily absolute of net radiation for the Bayelva/Tianshuihai simulations. As no hydrological simulations were run for the Tianshuihai site, no mass balance is given here.

4   Model set up

The thermal and hydraulic parameters used in this study were obtained by manual optimiziation of initial estimates based on previous analyses by Roth and Boike (2001) and are given in Table 1. To obtain the parameters of the freezing characteristics, the measured freezing curves were plotted (Fig. 4), and a manual fit with $\theta_w = \phi$ was put into measurements from probes situated in the water saturated section of the profile. The values were then varied by some percent such that the simulated temperatures and water contents within the whole profile fit the measurements in a better way. The solid line in Fig. 4 shows the optimized function.

For the Bayelva site we used homogeneous thermal properties for the complete soil profile. The heat conductivity of the soil material $K_{h_{soil}}$ was obtained by manual optimization, while the heat capacity C_{soil} was taken from Roth and Boike (2001). The quantity that determines heat conduction is the thermal diffusivity D_h ($m^2 s^{-1}$), which is defined as the ratio K_h/C_{eff}, where C_{eff} ($J m^{-3} K^{-1}$) is the effective soil heat capacity that can be obtained by averaging the heat capacities of the components (solid matrix, air, water and ice), weighed by their respective volume fractions.

To examine the influence of heat convection by liquid water and water vapor compared to heat conduction, three scenarios with different complexity of the model of the Bayelva site were run as given in Table 2. The most complex scenario (i) includes conductive as well as convective heat transport by liquid water and water vapor, scenario (ii) is the same discarding water vapor transport, while scenario (iii) considers conductive heat transport only. Each run was performed with the same set of parameters, which was manually optimized for the most complex scenario (i).

Unlike at the Bayelva site, the data from the Tianshuihai site has not been analyzed in previous studies. Also, as no texture analysis was performed, most material properties had to be estimated from textural information based on field observations. As we will discuss in Sect. 5.2, hydraulic processes were switched off, so only scenario (iii) was analyzed for the Tianshuihai site.

Test runs of the simulation with a homogeneous medium provided unsatisfactory results, with temperature deviations between measured and simulated data of more than 3 ˚C. As the soil shows a quite pronounced layering and its texture strongly changes with depth, the modeled domain was separated into three layers with boundaries at depths of 0.13 m and 0.97 m with different heat conductivities $K_{h_{soil}}$. All other parameters were kept constant over the spatial domain.

Parameters were adapted using an approach that alternates automatic estimation for adjustment of the three different heat conductivities $K_{h_{soil}}$ in the different layers and manual optimization of all other parameters. The automatic estimation was done by rastering the parameter space, running forward simulations for a discrete set of values for each parameter, with an increased maximum time step of 3 h for computational speed. The optimal parameter sets for both sites were determined by the minimal sum of squared differences between the measured and the simulated values. This method accounts for the observation that a homogeneous soil did not provide satisfactory results, while an inversion of all parameters was not conceivable computationally. The heat capacity will only influence the values we obtain for $K_{h_{soil}}$, but not the simulated temperature distribution, because the heat equation only depends on the thermal diffusivity D_h. Resulting values are given in Table 1.

4.1 Boundary and initial conditions

For the upper boundaries we used the soil temperature and water content measurements of the uppermost temperature and TDR probes to drive the model. This resulted in boundary fluxes that were highly dependent on the soil hydraulic and thermal properties. If we now obtain good agreements between measured and simulated data, we claim that the fluxes are in good accordance with the measurements and that we thus have obtained reasonable parameters.

For soil temperatures below 0 ˚C we used the last soil water content from temperature measurements above freezing as total water content for the upper forcing. This was necessary because we could not use the TDR measurements for the total soil

water content in winter, as they only return the liquid water content, while we needed the total (frozen and unfrozen) water content as upper boundary condition. Due to the low hydraulic conductivity and the presumed low water vapor fluxes in frozen grounds, this assumption should be valid, only when rain occurs shortly after freezing starts,
5 water infiltration might be underestimated.

Because of the permafrost below the modeled domain, we assumed that no water moves through the lower boundary. For the modeling the thermal lower boundary condition, in natural soils there is no physically obvious choice anywhere close to the modeled domain. As we do have temperature measurements within the profile, we
10 used these as the lower boundary condition. While it would be desirable to use a lower boundary in greater depth where temperatures stay constant, our approach enabled us to calibrate the model by adjusting the soil hydraulic and thermal parameters, and allowed to identify structural deviations between the simulation and the measured data.

As initial conditions for the heat equation we applied a linear interpolation between
15 the measured temperature values. For the water contents, we apply a temporal average of measured soil water contents in summer, because the model is initialized when at least parts of the soil are frozen. At greater depth, where the soil does not thaw completely in summer and thus total water contents could not be measured, we used measurements from the TDR probe right above the permafrost table, assuming that the
20 total soil water content stays constant below this depth. Between the sensors, linearly interpolated values were used. As the water content in general is not a continuous quantity, these values might not actually represent the stationary problem, but should be close to a solution if the model represents reality well, and thus equilibrate quickly.

5 Results

25 The results for the most complex scenario (i) of the simulation of the Bayelva site with conductive and convective heat transport through liquid water and water vapor is shown in Fig. 5, characteristic features of all scenarios of the Bayelva simulation are provided

in Fig. 7. Results of the Tianshuihai simulation are provided in Figs. 6 and 8. The largest observed temperature deviations between measured and simulated values in the different scenarios are shown in Table 3.

In all simulations, the qualitative accordance between the measured and the simulated values is reasonably good, typical features found in permafrost soils are represented: the low temperatures during the cold periods in winter, the warming periods that end with sharp thawing fronts propagating into the soils in late spring, the thawed periods, and finally the zero curtains, isothermal plateaus and the subsequent cooling periods. In general, the shape of the isotherms in the measured data and in the simulations as well as the shapes of the water content plots agree reasonably well.

From the values given in Table 3 and Fig. 5 we can see that at the Bayelva site winter temperatures are generally reproduced very well, with the absolute error being larger in the second winter than in the other winters. This can be explained by the lower snow cover, which leads to a weaker insulation from the cold air and thus lower temperatures within the soil, causing a larger absolute error when the relative error is similar. Also, in the fall of 1999 we observed strong rain events shortly after freezing starts, which lead to infiltration into an already frozen ground in the simulation, and thus an overestimation of the ice content in winter. In scenario (ii) of the Bayelva site, where convection by water vapor is excluded, we obtain almost identical results as in scenario (i), where vapor transport is considered (see Fig. 7). While the temperatures in scenario (iii) with heat conduction only differ by less than 0.2 °C from the first two scenarios, we could observe that the isothermal plateau is about three days longer than in the first two scenarios, and about two days closer to the measurements.

At the Bayelva site, due to the additional heat transport process the isothermal plateau ends five days earlier in the scenarios that include convective transport (i and ii), while for scenario (iii) with conduction only predictions are fairly good for both sites, with deviations of mostly less than two days (see Figs. 7 and 8).

The thaw depth estimate is quite good in all scenarios, which is to be expected due to the nearby temperature forcing at the lower boundary. However, we can observe

that the thawing front is up to two weeks slower, yet propagating about five centimeters deeper than in the measured data at both sites and in all scenarios. This fits well with the observed underestimation of the temperatures in early summer: due to the large amount of latent heat at the thawing front, the movement of the front is slow compared to the diffusive heat transport processes above, so the thawing front imposes a lower boundary to the heat conduction problem in the thawed regime. If this boundary is not as deep as in reality, we will underestimate the temperatures above it. Possible reasons for this effect are discussed in Sect. 6.2.

5.1 Heat transport processes

The mean heat fluxes in the observed profile for the Bayelva site are shown in Fig. 9 in order to illustrate the relative importance of the corresponding transport mechanisms. Heat transport is dominated by conduction in all simulated scenarios. In the unfrozen regime, heat transport by liquid water convection contributes with 3.2% to the total heat flux, while for very short periods during rain events it can reach almost 100% in the upper layers. Contributions by water vapor can be observed in summer as well as in winter, but its contribution is very low with 0.01% during summer and 0.03% throughout the year. In the upper 0.05 m, they are somewhat larger with 0.03% during summer and 0.2% throughout the year. At the Tianshuihai site, we did not model convective transport, the results presented here are based on the heat conduction scenario (iii).

5.2 Hydraulic effects

In the scenarios that include hydraulic processes (Bayelva, scenarios (i) and (ii)), the water movement in summer is represented fairly well, the liquid soil water contents deviate by less than 0.05 during most of the time. For short periods during the phase transitions, the error increases to at most 0.25, corresponding to energy defects of up to 10 MJ m^{-2}, because the time of freezing or thawing does not fit exactly. In contrast, at the Tianshuihai site, no hydraulic parameters could be found at which no massive infiltration of water during the first summer occurs in the simulation when we include

the hydraulic equations. There are several reasons for this: first, potential evaporation is about 20 to 50 times higher than precipitation (Gasse et al., 1991), so rain that evaporates below the uppermost TDR probe will stay in the modeled system, because vapor flow across the boundary is not implemented. Also, even small overestimations of the water contents in the TDR measurements, which may occur at this site due to high salt contents close to the soil surface, can lead to massive infiltration especially in the dry regime, because the water flux at the upper boundary is obtained from the TDR measurements and the hydraulic conductivity, which is highly non-linear. Except for two rain events in the summer of 2008, the assumption that convective transport does not play an important role at the Tianshuihai site is also supported by the TDR measurements, which show an almost constant water content within the soil with a water table that varies only by a few centimeters during the unfrozen period. Due to these methodological problems, the scenarios (i) and (ii) of the Tianshuihai simulation have not been further analyzed.

5.3 Inhomogeneity effects

While at both sites the soil consists of different layers, the simulation with homogeneous soil parameters returned good results for the Bayelva site, while temperature predictions differed significantly from measured values at the Tianshuihai site. At the Bayelva site, the transition between the layers is smooth, while at the Tianshuihai site, we have very distinct layer boundaries.

As shown in Table 1, the estimated heat conductivity $K_{h_{soil}}$ in the upper 0.13 m of the Tianshuihai profile is very small. As this layer is very dry with water contents of 0.05 to 0.08, with peaks reachig 0.16 during rain events, there is almost no water present at the contact interfaces of the soil particles, so the de Vries model which determines the effective heat conductivity K_h from the heat conductivities and volume fractions of the soil constituents will not be accurate. The algorithm that determines the heat conductivities in the different layers will adjust the only free parameter $K_{h_{soil}}$ such that it returns a reasonable effective parameter K_h.

6 Discussion

We modeled processes in the active layer at two sites that show rather different surface as well as subsurface structures, and are subject to highly different atmospheric forcing. We were able to reproduce the thermal dynamics at both sites, relevant processes are sufficiently similar to be represented by the same mathematical model, although the inclusion of site specific knowledge such as atmospheric conditions, surface structure and subsurface texture is crucial for a model setup that enables a correct representation. Including this knowledge together with measured temperature and TDR data, it was possible to obtain reasonable values for all parameters. For the thermal diffusivity D_h in the frozen regime in 1998/1999 at the Bayelva site, Roth and Boike (2001) obtained $0.8 \times 10^{-6} \, \mathrm{m^2 \, s^{-1}}$. Values used in this work change over time and range from $1 \times 10^{-6} \, \mathrm{m^2 \, s^{-1}}$ to $1.4 \times 10^{-6} \, \mathrm{m^2 \, s^{-1}}$, depending on the soil composition. For comparison with the previously obtained value, we artificially decreased D_h by a factor of 1.5, leading to values between $0.67 \times 10^{-6} \, \mathrm{m^2 \, s^{-1}}$ and $0.93 \times 10^{-6} \, \mathrm{m^2 \, s^{-1}}$. This increased the error by up to $0.06\,°C$ in the first and third winter, and by up to $0.2\,°C$ in the second. Differences in thaw depth were well below $0.01\,m$, so we claim reasonable accordance between these manually adjusted parameters. In the following, we will discuss some specific requirements needed for good performance of the model.

6.1 The layered model

While at the Bayelva site we obtained reasonable results with a homogeneous model, we needed a layered model at the Tianshuihai site. This could be because of the very dry layer at the top, which by failure of the de Vries model leads to an unphysical effective soil heat conductivity $K_{h_{soil}}$ in this region, as this is the only free parameter in determining the thermal diffusivity. Due to the very low water content, the very dry top layer at the Tianshuihai site also has an effective thermal diffusivity that differs from the rest of the soil, which matches the observation that it is important to include strongly differing thermal diffusivities even in a small layer.

Another possible explanation for the necessity to include a layered model could be large scale ground water flow in the deeper part of the active layer. However, due to the flat topography and presumably very similar thermal properties throughout the plain, we expect very similar thaw depths everywhere and thus no significant ground water flow above the frost table.

6.2 Temperature and thaw depth deviations in summer

At both sites, the most significant deviation between the measured and the simulated data is the underestimated heat entry in early summer. In a two dimensional model simulating conductive heat transport, Kane et al. (1991) observed similar deviations for a study site near Toolik Lake, Alaska, underestimating the temperature in spring by at most 1 °C. While they attribute this to convective contributions to heat transport, we cannot simply make this assumption for the Bayelva site, because these processes are included in the model. Possible explanations have to consider that it has to be either an effect which is not detected by the uppermost temperature sensor or a non-diffusive process. In addition, we need explanations for a very similar effect at both sites, although the deviations are about twice as strong at the Bayelva site than at the Tianshuihai site.

In the fall of 1999, at the Bayelva site we observed strong rain events shortly after freezing starts, which lead to infiltration into an already frozen ground in the simulation, and thus an overestimation of the ice content in winter. This might be one of the reasons for the underestimation of the thaw depth in the following summer in scenarios (i) and (ii) and the resulting underestimation of temperatures in the unfrozen regime. However, as the temperature is also underestimated in the heat conduction scenario (iii) at both sites in all summers, there must be another effect involved in causing the observed deviations. In the following, we will discuss downward vapor migration through dry cracks and mechanical soil expansion as possible explanations.

While we could not simulate water migration for the Tianshuihai site, some effects of the rain can be observed in the temperature estimates: in the summer of 2008,

two distinct infiltration events can be identified in the TDR data (Fig. 6b, 8 July and 5 August to 16 August), and during these times the error in the temperature estimation increases significantly, such that temperatures are underestimated by the simulation. As evaporation from the surface is implicitly included in the upper boundary, this hints towards either an increase of the effective thermal conductivity by the additional water, convection of rain water that is warmer than the soil or subsurface evaporation from below the uppermost sensors. The failure of the model that includes convection at the Tianshuihai site does not allow for an analysis of surface or subsurface evaporation. Also, rain events during these periods occur about evenly distributed over the times of the day, and no reliable rain measurements are available, so we cannot ascertain which of these processes are dominantly causing the temperature differences.

6.2.1 Dry cracking and water vapor condensation

One possible explanation for the underestimation of the heat entry in early summer would be dry cracking, which was observed at the Bayelva site on top of the mud boils. Within these cracks, air convection could transport large amounts of heat from the surface below the upper temperature sensor. CO_2-concentration measurements in an adjacent mud boil show that gas exchange can occur down to 0.73 m depth (B. Hagedorn, unpublished data). On 15 July 1999 a decrease in CO_2 was observed for which pure diffusion can be excluded. The starting of the underestimation of summer temperatures at this time is a hint that dry cracking could be responsible for the deviations.

At the Tianshuihai site in contrast, the only cracks observed were larger cracks filled with sand wedges and reaching to a depth of about 0.3 m. Additional smaller cracks are unlikely, considering the coarse grained surface sediments.

As we have shown for the Bayelva site, the amount of heat transported by convection of water vapor within the soil is two orders of magnitude smaller than heat convected by liquid water. However, the way vapor transport was implemented in this model, vapor flow across the upper boundary is not included, so it would be possible that vapor

from above the upper boundary infiltrates into the soil through cracks and deposits its latent heat below the uppermost temperature probe. Due to the temperature gradient between the atmosphere and the soil surface, this effect would preferably occur around July, when air temperatures are high. This is also the time at which the thaw depth is underestimated most.

In contrast, condensation at the surface cannot be responsible, as it is implicitly included in the way the boundaries are implemented. Outcalt et al. (1998) have shown for a study site in Alaska that evaporation from within the upper few centimeters of the soil can cool the active layer by several degrees. This shows that vapor transport within the upper soil layers can have a significant impact, although we would need the effect to be in the opposite direction to explain the observed differences.

A rough estimate illustrates the dimensions that the latent heat deposition within the cracks would need to have: with an effective soil heat capacity of $2.4 \times 10^6 \, \mathrm{J\,m^{-3}\,K^{-1}}$ (as given by Roth and Boike (2001)), a condensation enthalpy of $2.5 \times 10^6 \, \mathrm{J\,kg^{-1}}$ and a thaw depth of $1/1.5\,\mathrm{m}$ for the Bayelva/Tianshuihai site, about $1.5/1.7\,\mathrm{kg\,m^{-2}}$ of water vapor would have to infiltrate into the soil within about one month at the beginning of the summer. With an average ice content of 0.3 and an underestimate in the thaw depth of $0.15/0.3\,\mathrm{m}$ in early summer, the latent heat needed corresponds to another $5.4/10.9\,\mathrm{kg\,m^{-2}}$ of vapor.

With typical values for air temperature of 5–$7/20\,^{\circ}\mathrm{C}$ and humidity of $80/50\%$ in July we obtain an absolute humidity of about $5.4/8.6\,\mathrm{g\,m^{-3}}$ compared to $4.8\,\mathrm{g\,m^{-3}}$ at the thawing front at $0\,^{\circ}\mathrm{C}$ and 100% relative humidity. This means that the water of about 4900–$11\,500/3300\,\mathrm{m^3}$ of air per square meter of soil surface would have to be deposited below the uppermost temperature probe within this period for the Bayelva/Tianshuihai site in order to account for the whole effect. Water that evaporates from below the uppermost probe must condensate in addition to this value, while evaporation from the surface is implicitly included in the simulations. Due to the low vapor diffusivity in soils, this seems impossible by vapor diffusion, while vapor convection through cracks could well be responsible.

6.2.2 Mechanical soil expansion

If we use realistic and thus temperature dependent values for the densities of liquid water and ice, we expect mechanical effects because of the low density of ice. In natural soils, this leads to an expansion of the soil as a whole. As these mechanical effects are not implemented in the model, the different densities can lead to unphysical effects: we observe a huge liquid phase gauge pressure that causes a rise of about 0.2 m in the water table during the isothermal phase and some small fluctuations during the frozen period. However, the water content distributions in summer as well as the temperature distributions do not change significantly in either scenario, because the total amount of water does not change. In real soils, the expansion of the soil matrix may lead to different distances between the probes in winter, because the probes have been installed in summer. If we now adjust the parameters such that the temperatures in winter are represented accurately, we will underestimate the thermal diffusivity and thus also the heat conductivity of the soil $K_{h_{soil}}$ in summer, because the distances in the simulated soil are smaller than in reality. This would lead to an underestimation of the temperatures as soon as they start to drop. However, this effect does not seem to be strong enough: as French (2007) states, the expansion of ice within the soil is directly converted into an expansion of the soil itself. The density of water is about 9% higher than the density of ice, which leads to an expansion of about 3% if we assume an average water content of 0.3 and a purely vertical expansion. Roth and Boike (2001) state that if we want to project a given temperature distribution into increasing depths we would have to increase the effective thermal diffusivity with the square of the depth to obtain the same distribution. In our case we would therefore have to increase the diffusivity by 6% to represent the temperature distributions in summer. However, test runs of the simulations showed that with this value the error of the temperature in summer improves, but only by about 0.03 °C. This is not sufficient to explain the observed differences.

7 Conclusions

We presented a coupled thermal and hydraulic model for the active layer dynamics and applied it to two rather different permafrost sites. By running different scenarios which included different heat transport processes we were able to show that at both sites heat transport is dominated by conduction, and that qualitatively, the thermal dynamics could be represented reasonably well with a model that considers conductive transport only. However, for a more accurate description it was necessary to include information about the respective site. Especially subsurface information about soil layering with good estimates of the thermal diffusivity in the respective layers showed to be important at the Tianshuihai site, where the hydraulic processes could not be represented with a parameterized model due to the very dry top layer. At the Bayleva site, convective transport by liquid water could be represented and does improve the thaw depth and temperature estimates, although the estimate of the length of the zero curtain became worse by some days. Heat convection by water vapor diffusion through the pore space does not contribute significantly at either site.

Although some layering is present at the Bayelva site, it was possible to represent the thermal dynamics reasonably well with a homogeneous model, while convective transport by liquid water does have a significant impact. However, as we showed for the Tianshuihai site, even with detailed knowledge about surface properties, thaw depth predictions may fail if significant layering is present.

Much research has been performed on the implementation of appropriate boundary conditions (e.g., Hinzman et al., 1998). In our study, we focussed on the processes within the soil, which was possible because in depth measurements were available for both sites and provided a way of avoiding surface parameterizations and guesses of temperature distributions below the modeled domain. Using daily averaged soil temperatures and soil water contents as exterior forcing showed to be sufficient for a detailed representation of temperature distributions and thaw depths.

References

Bittelli, M., Ventura, F., Campbell, G., Snyder, R., Gallegati, F., and Pisa, P.: Coupling of heat, water vapor, and liquid water fluxes to compute evaporation in bare soils, J. Hydrol., 362, 191–205, 2008. 239, 240

Boike, J., Roth, K., and Ippisch, O.: Seasonal snow cover on frozen ground: Energy balance calculations of a permafrost site near Ny-Ålesund, Spitsbergen, J. Geophys. Res., 108(D2), 8163, doi:10.1029/2001JD000939, 2003. 233

Boike, J., Ippisch, O., Overduin, P., Hagedorn, B., and Roth, K.: Water, heat and solute dynamics of a mud boil, Spitsbergen, Geomorphology, 95, 61–73, 2008. 233

Buck, A.: New equations for computing vapor pressure and enhancement factor, J. Appl. Meteorol., 20, 1527–1532, 1981. 240

Carslaw, H. and Jaeger, J.: Conduction of heat in solids, chap. XI, Oxford University Press, 2nd edn., 287–288, 1959. 240

COMSOL Multiphysics: Version 3.5a, 03.12.2008, http://www.comsol.com/, 2008. 240

Daanen, R., Misra, D., and Epstein, H.: Active-layer hydrology in nonsorted circle ecosystems of the Arctitc Tundra, Vadose Zone J., 6, 694–704, 2007. 231

de Vries, D.: Transfer processes in the Plant Environment, in: Heat and Mass Transfer in the Biosphere, Wiley and Sons, New York, 5–28, 1975. 238

Engelmark, H. and Svensson, U.: Numerical modelling of phase change in freezing and thawing unsaturated soil, Nord. Hydrol., 24, 95–110, 1993. 231

French, H.: The Periglacial Environment, Wiley, 3rd edn., 2007. 230, 251

Gasse, F., Arnold, M., Fontes, J., Fort, M., Gibert, E., Huc, A., Bingyan, L., Yuanfang, L., Qing, L., Melieres, F., Campo, E. V., Fubao, W., and Qingsong, Z.: A 13 000-year climate record from Western Tibet, Nature, 353, 742–745, 1991. 246

van Genuchten, M.: A closed-form equation for predicting the hydraulic conductivity of unsaturated soils, Soil Sci. Soc. Am. J., 44, 892–898, 1980. 236

Guymon, G. and Luthin, J.: A coupled heat and moisture transport model for arctic soils, Water Resour. Res., 10, 995–1001, 1974. 231, 232, 236

Hansson, K., Šimůnek, J., Mizoguchi, M., Lundin, L., and van Genuchten, M.: Water flow and heat transport in frozen soil: numerical solution and freeze-thaw applications, Vadose Zone J., 3, 693–704, 2004. 236

Harlan, R.: Analysis of coupled heat-fluid transport in partially frozen soil, Water Resour. Res., 9, 1314–1323, 1973. 231

Harris, K., Haji-Sheikh, A., and Nnanna, A. A.: Phase-change phenomena in porous media – a non-local thermal equilibrium model, Int. J. Heat Mass Tran., 44, 1619–1625, 2001. 231

Hinzman, L., Goering, D., and Kane, D.: A distributed thermal model for calculating soil temperature profiles and depth of thaw in permafrost regions, J. Geophys. Res., 103, 28975–28991, 1998. 231, 236, 252

Ippisch, O., Cousin, I., and Roth, K.: Wärmeleitung in porösen Medien – Auswirkungen der Bodenstruktur auf Wärmeleitung und Temperaturverteilung, Mitteilgn. Dtsch. Bodenkundl. Gesellsch., 87, 405–408, 239

Javierre, E., Vuik, C., Vermolen, F., and van der Zwaag, S.: A comparison of numerical models for one-dimensional Stefan problems, J. Comput. Appl. Math., 192, 445–459, 2006. 231

Kane, D., Hinzman, L., and Zarling, J.: Thermal response of the Active layer to climatic warming in a permafrost environment, Cold Reg. Sci. Technol., 19, 111122, 1991. 248

Kane, D., Hinkel, K., Goering, D., Hinzman, L., and Outcalt, S.: Non-conductive heat transfer

associated with frozen soils, Global Planet. Change, 29, 275–292, 2001. 231

Li, S. and He, Y.: Features of permafrost in the West Kunlun Mountains, Bull. Glacier Res., 7, 161–167, 1989. 234

Mualem, Y.: A new model for predicting the hydraulic conductivity of unsaturated porous media, Water Resour. Res., 12, 593–622, 1976. 237

Nakano, Y. and Brown, J.: Effect of a Freezing Zone of Finite Width on the Thermal Regime of Soils, Water Resour. Res., 7, 1226–1233, 1971. 231

Outcalt, S., Hinkel, K., Nelson, F., and Miller, L.: Estimating the magnitude of coupled-flow effects in the Active layer and upper permafrost, Barrow, Alska, USA, in: Proceedings of the 7th International Permafrost Conference, Yellowknife, Canada, Collection Nordicana, 55, 869–873, 1998. 250

Philip, J.: Evaporation, and moisture and heat fields in the soil, J. Meteorol., 14, 354–366, 1957. 240

Riseborough, D., Shiklomanov, N., Etzelmüller, B., Gruber, S., and Marchenko, S.: Recent advances in permafrost modelling, Permafrost Periglac., 19, 137–156, 2008. 231

Romanovsky, V. and Osterkamp, T.: Thawing of the ActivelLayer on the coastal plain of the Alaskan Arctic, Permafrost Periglac., 8, 1–22, 1997. 231

Roth, K. and Boike, J.: Quantifying the thermal dynamics of a permafrost site near Ny-Ålesund, Svalbard, Water Resour. Res., 37, 2901–2914, 2001. 232, 233, 241, 247, 250, 251

Šimůnek, J., Huang, K., and Genuchten, M. V.: The SWMS_3D code for simulating water flow and solute transport in three-dimensional variably-saturated media, Version 1.0, Research Report No. 139, US Salinity Laboratory, Agricultural Research Service, US Department of Agriculture, Riverside, California, 1995. 240

Weischet, W.: Einführung in die Allgemeine Klimatologie, Teubner Studienbücher, 5 edn., 1991. 239

Modeling thermal dynamics of active layers

J. Weismüller et al.

Title Page

Abstract | Introduction

Conclusions | References

Tables | Figures

◄◄ | ►►

◄ | ►

Back | Close

Full Screen / Esc

Printer-friendly Version

Interactive Discussion

Table 1. Soil parameters used in the simulations. As no convective flow has been modeled for the Tianshuihai site, no Mualem-van Genuchten parameters were necessary.

Parameter		Bayelva	Tianshuihai
Freezing curve	a	8×10^{-2}	4×10^{-2}
	c	8×10^{-4}	8×10^{-4}
	d	9×10^{-2}	9×10^{-2}
Hydraulic properties	ϕ	0.42	0.39
	α	$1.8\,\mathrm{m}^{-1}/(\rho_\mathrm{l}\,g)$	
	n	1.5	
	θ_r	0	
	κ	$2\times10^{-12}\,\mathrm{m}^2$	
Thermal properties	C_soil	$1.95\times10^6\,\mathrm{J\,m}^{-3}\,\mathrm{K}^{-1}$	$2.5\times10^6\,\mathrm{J\,m}^{-3}\,\mathrm{K}^{-1}$
	$K_\mathrm{h_{soil}}$	$3.8\,\mathrm{W\,m}^{-1}\,\mathrm{K}^{-1}$	$1.0\,\mathrm{W\,m}^{-1}\,\mathrm{K}^{-1}$ (above 0.13 m)
			$2.2\,\mathrm{W\,m}^{-1}\,\mathrm{K}^{-1}$ (0.13–0.97 m)
			$3.4\,\mathrm{W\,m}^{-1}\,\mathrm{K}^{-1}$ (below 0.97 m)

Modeling thermal dynamics of active layers

J. Weismüller et al.

Table 2. Simulation scenarios.

(i)	Conductive as well as convective heat transport by liquid water and water vapor Using all processes that are described by Eqs. (1) to (17)
(ii)	Conductive as well as convective heat transport by liquid water Omitting Eqs. (11) to (17)
(iii)	Conductive heat transport only, assuming a variably saturated soil Omitting Eqs. (1), (5) and (11) to (17), and setting $j_w = 0$

Table 3. Maximal temperature deviations between simulated and measured data.

Scenario	Bayelva Winter	Bayelva Summer	Tianshuihai Winter	Tianshuihai Summer
(i), (ii) and (iii) at Bayelva, (iii) at Tianshuihai	0.6 °C in 1998/1999 1.0 °C in 1999/2000 0.4 °C in 2000/2001	2.1 °C	1.0 °C in 2008/2009	1.6 °C in 2008 0.8 °C in 2009

Table 4. List of symbols.

a, b, c and d	Parameters caracterizing the freezing curve (–)
C_g	Molar heat capacity of the gas ($\text{J mol}^{-1}\,\text{K}^{-1}$)
C_i	Molar heat capacity of ice ($\text{J mol}^{-1}\,\text{K}^{-1}$)
C_l	Molar heat capacity of liquid water ($\text{J mol}^{-1}\,\text{K}^{-1}$)
C_{soil}	Volumetric heat capacity of the soil matrix ($\text{J m}^{-3}\,\text{K}^{-1}$)
c_v	Molar concentration of water vapor (mol m^{-3})
c_w	Molar concentration of water with respect to the entire volume (mol m^{-3})
D_0	Reference water vapor diffusivity ($\text{m}^2\,\text{s}^{-1}$)
D_g	Water vapor diffusivity ($\text{m}^2\,\text{s}^{-1}$)
D_h	Thermal diffusivity ($\text{m}^2\,\text{s}^{-1}$)
E	Thermal energy density (J m^{-3})
g	Gravitational acceleration ($\text{m}^2\,\text{s}^{-1}$)
h_r	Relative humidity (–)
j_e	Energy flux (W m^{-2})
j_g	Molar vapor flux ($\text{mol m}^{-2}\,\text{s}^{-1}$)
j_w	Total water flux ($\text{mol m}^{-2}\,\text{s}^{-1}$)
K_h	Heat conductivity ($\text{W m}^{-1}\,\text{K}^{-1}$)
K_l	Liquid phase conductivity ($\text{m}^3\,\text{s kg}^{-1}$)
k_t	Form factors (–)
L_f	Latent heat of freezing (J mol^{-1})
L_v	Latent heat of vaporization (J mol^{-1})
M_w	Molar mass of water (kg mol^{-3})
m	van Genuchten shape parameter (–)
n	van Genuchten shape parameter (–)
p_{atm}	Atmospheric pressure (Pa)
p_w	Water pressure [Pa]
R	Universal gas constant ($\text{J mol}^{-1}\,\text{K}^{-1}$)
s	Slope of the saturation vapor concentration ($\text{mol m}^{-3}\,\text{K}^{-1}$)
T	Temperature (°C)
α	van Genuchten scaling parameter (Pa^{-1})
θ_g	Volume fraction occupied by gas (–)
θ_i	Volumetric ice content (–)
θ_l	Volumetric liquid water content (–)
θ_r	Residual water content (–)
κ	Hydraulic permeability (m^2)
μ_l	Dynamic viscosity of liquid water (Pa s)
v_g	Molar density of the gas (mol m^{-3})
v_i	Molar density of ice (mol m^{-3})
v_l	Molar density of liquid water (mol m^{-3})
ϕ	Porosity (–)
ρ_i	Mass density of ice (kg m^{-3})
ρ_l	Mass density of liquid water (kg m^{-3})

Bayelva

Tianshuihai

Fig. 1. Locations of the study sites.
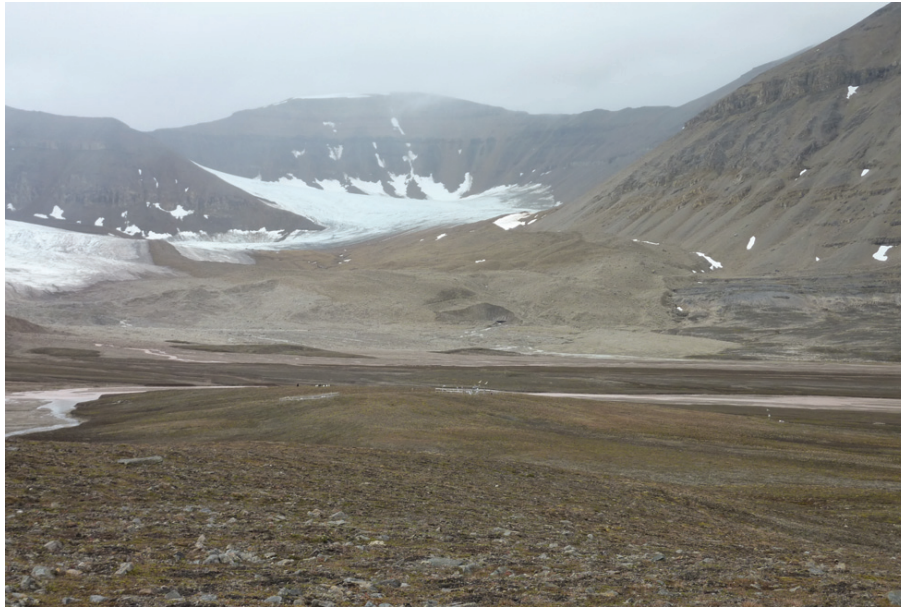
Fig. 2. View over the Bayelva catchment area.

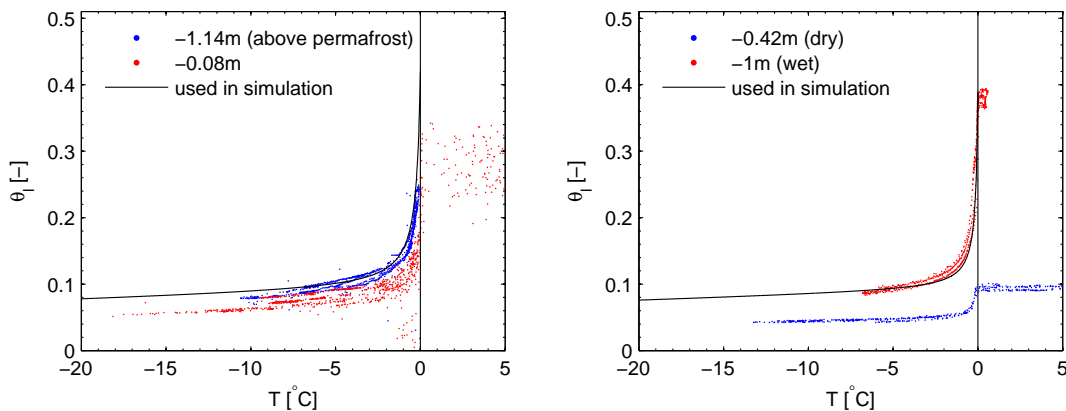**Fig. 3.** Overview over the sedimentary plain at the Tianshuihai station.

Fig. 4. Measured soil freezing characteristics and manually adapted fits for $\theta_w = \phi$. Left: Bayelva, right: Tianshuihai.
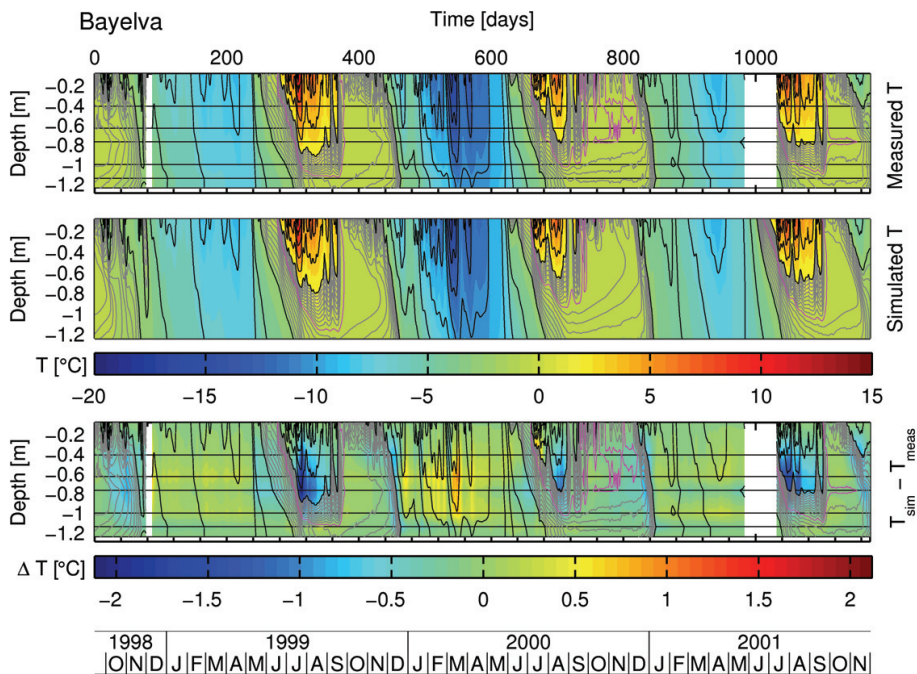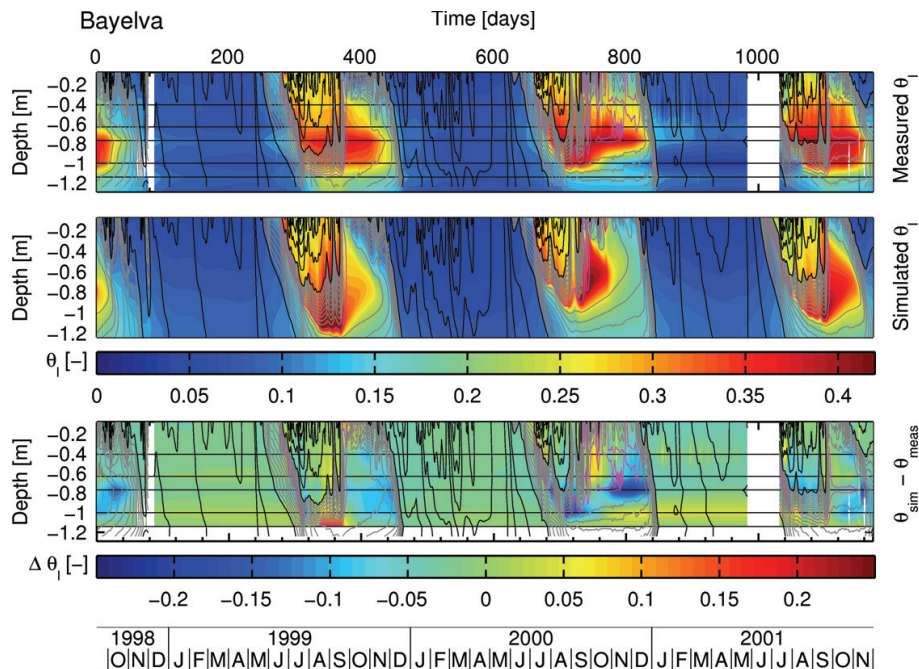
Fig. 5a. Measured and simulated soil temperatures for the Bayelva simulation with conductive and convective transport by liquid water and water vapor (scenario (i)). Top two: Measured and simulated soil temperatures, with solid lines every 2 °C, gray lines every 0.2 °C between –2 °C and 2 °C and a magenta line for 0 °C. Bottom: Simulated minus measured temperatures, with the measured temperature lines repeated for cross referencing. Horizontal lines represent the sensor positions.

Fig. 5b. Measured and simulated soil water contents for the Bayelva simulation with conductive and convective transport by liquid water and water vapor (scenario (i)). Top two: Measured and simulated liquid soil water contents, with the lines from the temperature plots (a) repeated. Bottom: Simulated minus measured water contents, with the measured temperature lines repeated for cross referencing. Horizontal lines represent the sensor positions.

Fig. 6a. Measured data and simulation results for the conduction scenario (iii) of the Tianshuihai simulation. Top two: Measured and simulated soil temperatures, with solid lines every 2 °C, gray lines every 0.2 °C between −2 °C and 2 °C and a magenta line for 0 °C. Bottom: Simulated minus measured temperatures, with the measured temperature lines repeated for cross referencing. Horizontal lines represent the sensor positions.
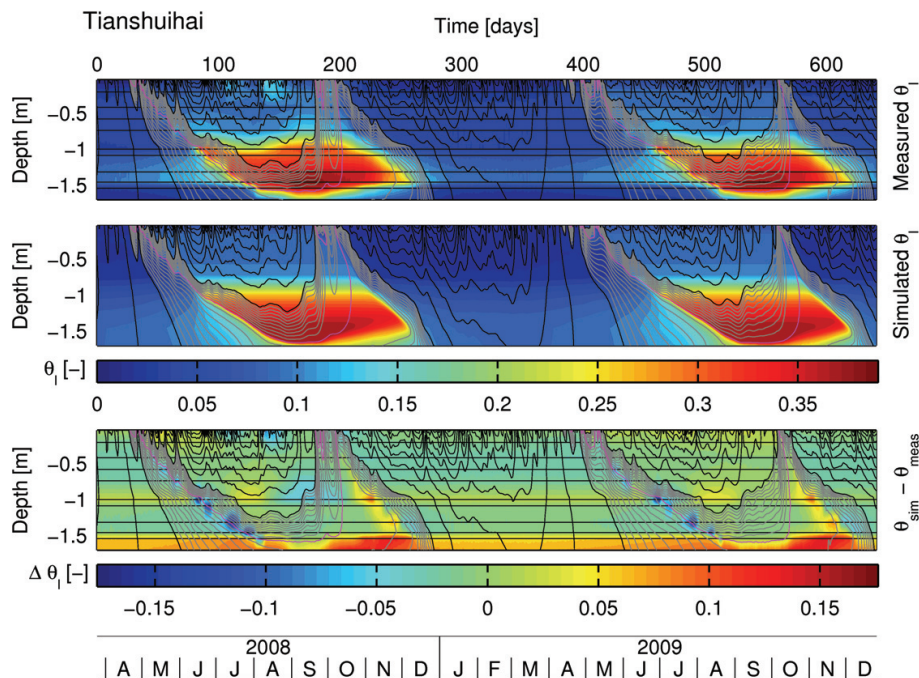
Fig. 6b. Measured and simulated soil water contents for the conduction scenario (iii) of the Tianshuihai simulation. Top two: Measured and simulated liquid soil water contents, with the lines from the temperature plots (a) repeated. Bottom: Simulated minus measured water contents, with the measured temperature lines repeated. Horizontal lines represent the sensor positions.

Full Screen / Esc
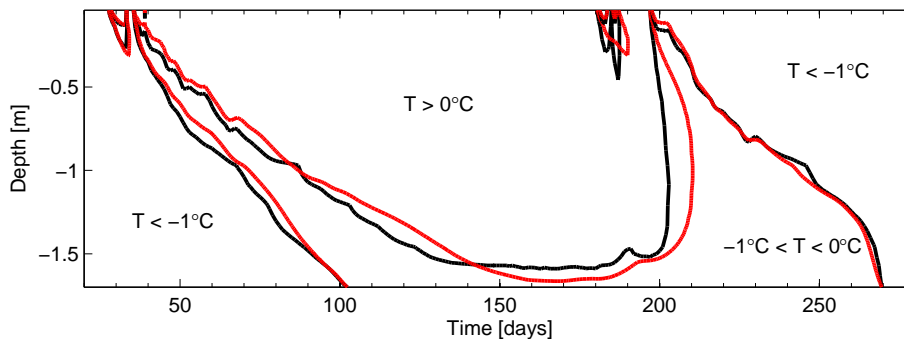
Printer-friendly Version

Interactive Discussion
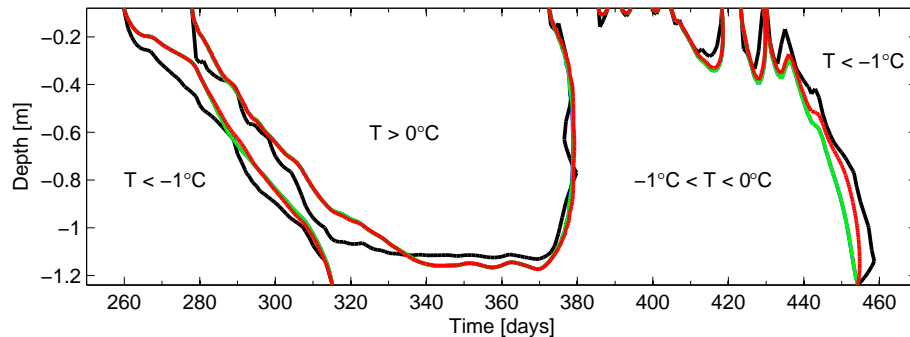
Fig. 7. Simulation results for the different scenarios at the Bayelva site in the summer of 1999. Shown are the 0°C and the −1°C isotherms. The colors represent: Black: Measured data, blue: Conduction with convection of liquid water and water vapor (i), green: Conduction with convection of liquid water (ii), red: Conduction with constant water distribution (iii). Blue (i) and green (ii) overlap almost entirely.

Fig. 8. Simulation results for the different scenarios at the Tianshuihai site in the summer of 2008. Shown are the 0 ˚C and the −1 ˚C isotherms. The colors represent: Black: Measured data, red: Conduction with constant water distribution (iii).
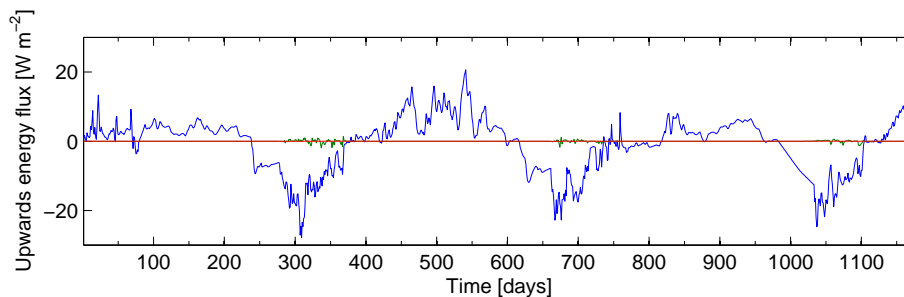
Fig. 9. Mean energy flux at the Bayelva site averaged over the depth of the profile. Blue: conductive, green: convective by liquid water, red: convective by water vapor.